Domain Wall Manipulation with a Magnetic Tip

T. Stapelfeldt, R. Wieser, E. Y. Vedmedenko, and R. Wiesendanger

Institute of Applied Physics and Microstructure Advanced Research Center, University of Hamburg, Jungiusstraße 11, D-20355 Hamburg, Germany

(Received 3 February 2011; published 7 July 2011)

A theoretical concept of local manipulation of magnetic domain walls is introduced. In the proposed procedure, a domain wall is driven by a spin-polarized current induced by a magnetic tip, as used in a scanning tunneling microscope, placed above a magnetic nanostripe and then moved along its long axis with a current flowing through the vacuum barrier. The angular momentum from the spin-polarized current exerts a torque on the magnetic moments underneath the tip and leads to a displacement of the domain wall. Particularly, the manipulation of a ferromagnetic 180° transverse domain wall has been studied by means of Landau-Lifshitz-Gilbert dynamics and Monte Carlo simulations. Different relative orientations of the tip and the sample magnetization have been considered.

DOI: 10.1103/PhysRevLett.107.027203 PACS numbers: 75.75.−c, 75.60.Ch, 75.78.Fg

Recent exciting developments towards new storage and logic devices are based on the current- and field-driven motion of magnetic domain walls (DWs) [1–3]. To read or write a bit of information, a DW has to be moved towards the reading or writing device. However, neither external fields nor currents allow us to address each DW individually. A spin-polarized current moves neighboring DWs in the same direction, while a magnetic field moves them in opposite directions. Up to now, the manipulation of a DW has been achieved by the stray field emanating from a tip of a magnetic force microscope (MFM) [4,5]. The best resolution of the MFM experiments is of the order of 20 nm [5]. The goal of our investigation is the manipulation of narrow DWs of width ≤ 2 nm in nanowires of monolayer thickness, which is about 1 order of magnitude smaller than that of walls in soft magnetic materials [4,5]. For that purpose we propose to address magnetic DWs individually using the spin torque [6–8] induced by a tip of a spin-polarized scanning tunneling microscope (SP-STM) [6]. We demonstrate theoretically that this technique allows controlled manipulation and subsequent imaging of atomically sharp DWs in nanoscale magnetic wires. SP-STM is applicable to a very broad class of conducting and semiconducting materials, and many different systems may be manipulated this way.

The influence of a SP-STM tip on a DW has been studied by means of the atomistic spin dynamics [Landau-Lifshitz-Gilbert (LLG)] as well as by Monte Carlo (MC) simulations. Several magnetization geometries have been analyzed. It is demonstrated that both approaches give reliable results and reveal the orientation of the tip magnetization parallel to the DW magnetization as the most promising geometry for future experimental applications.

In the simulations a ferromagnetic monolayer stripe with lateral dimensions of $40a \times 70a$, has been considered. Each site is occupied by a classical Heisenberg moment $\vec{S}_i = (S_i^x, S_i^y, S_i^z)$ of unit length $\vec{\mu}_i/\mu_s$. The magnetic properties are given by the following Hamiltonian:

$$\mathcal{H} = -J\sum_{\langle ij\rangle}\vec{S}_i\vec{S}_j - D_x\sum_i (S_i^x)^2 + D_z\sum_i (S_i^z)^2, \quad (1)$$

where $J > 0$ denotes the ferromagnetic exchange coupling between nearest neighbors, $D_x > 0$ is an easy axis and $D_z > 0$ a hard axis anisotropy. Hence, the rotation of magnetization is confined to the xy plane. The dipolar coupling of such an ultrathin in-plane system is small and has been neglected. Material parameters in the range typical for recently studied experimental systems [7] like Fe/W(110) or Co/Pt(111) monolayers have been used in the calculations ($J = 10$ meV, $D_x = 1.25$ meV, and $D_z = 0.5$ meV). For the spin dynamic calculations the motion of DWs has been described by the generalized Landau-Lifshitz-Gilbert equation

$$\frac{\partial\vec{S}_i}{\partial t} = -\frac{\gamma}{(1+\alpha^2)\mu_S}\vec{S}_i \times [\vec{H}_i + \alpha(\vec{S}_i \times \vec{H}_i)] + \mathcal{C}\vec{S}_i \times \vec{\mathcal{T}}_i + \mathcal{D}\vec{S}_i \times (\vec{S}_i \times \vec{\mathcal{T}}_i), \quad (2)$$

with the gyromagnetic ratio γ, the Gilbert damping $\alpha = 0.025$, the effective field $\vec{H}_i = -\partial\mathcal{H}/\partial\vec{S}_i$, and the spin current $\vec{\mathcal{T}}_i$. The last two terms are the contributions (precession and relaxation) of the spin torque [8]. The influence of the electric current is described similarly to the case of a spin valve [9–11] by $\mathcal{C} = 0.05$ and $\mathcal{D} = 1$. In the MC scheme the s-d model [12] has been used to account for the spin torque of tunneling electrons:

$$\mathcal{H}_{\mathcal{T}} = -g\sum_i \vec{\mathcal{T}}_i \cdot \vec{S}_i, \quad (3)$$

where g is the coupling constant. In the following we set g to unity, so that all of the information on the spin-polarized current is given by $\vec{\mathcal{T}}_i$.

In the low-bias regime the local strength and the orientation of the tunneling current is accurately described by the Tersoff-Hamann model [13]:

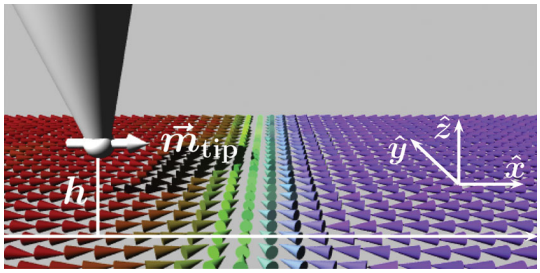

FIG. 1 (color). Scheme of a spin configuration of the sample. A DW elongated in $+y$ direction separates two domains. The spins in the domains point along the easy axis. A tip with a magnetization $\vec{m}_{\rm tip}$ and height h above the sample moves towards the DW along the indicated track in the $+x$ direction (white horizontal line).

$$\vec{\mathcal{T}}_i = -I_0 e^{-2\kappa\sqrt{(x_i-x_{\rm tip})^2+(y_i-y_{\rm tip})^2+h^2}} P \cdot \vec{m}_{\rm tip}, \qquad (4)$$

with the polarization P of the tip magnetization $\vec{m}_{\rm tip}$ (a unit vector in the direction of the tip magnetization), the inverse decay length of the wave function in vacuum κ, the time dependent tip and atom positions $\vec{r}_{\rm tip} = (x_{\rm tip}, y_{\rm tip}, h)$, $\vec{r}_i = (x_i, y_i, 0)$, and I_0 the spin-polarized current averaged over the surface unit cell. In the spin dynamic simulation we set $I_0^{\rm LLG} = 10^9 \frac{\mu_S}{\gamma J t}$, and in the MC procedure we set $I_0^{\rm MC} = 7.5 \times 10^4 \frac{\mu_S}{\gamma J}$ per Monte Carlo step (MCS). Parameter κ contains the work function ϕ of magnetic tip materials used in experiments ($\phi = 4.5$ eV for Cr). For the chosen sample and tip parameters we assume the spin torque acting on the magnetic moments to be large compared to Oersted fields and Joule heating [7,14], which have been neglected in our simulations.

A typical tip-wall configuration is shown in Fig. 1. The simulations have been started with a completely relaxed 180° transverse DW at low temperature to minimize thermal fluctuations ($T_{\rm LLG} = 0$ K, $T_{\rm MC} = 1$ K). The DW width obtained was of the order of 2 nm, in agreement with experiment [15]. For the sake of comparison with experiments, we were interested in the equilibrium DW motion. For that purpose an adequate tip step $\Delta x_{\rm tip}$ has been chosen for both simulation methods to ensure a full relaxation of the DW during manipulation. In the spin dynamic simulations we consider a constant tip velocity of $v_{\rm tip} = 1.5$ m/s. This velocity is higher than typical experimental values, but still sufficient for a proper sample relaxation. For the MC relaxation a standard METROPOLIS update algorithm has been implemented, resulting in a constant tip velocity of $v_{\rm tip} = 10^{-6}$ lattice constants per MCS.

The simulations have been performed for three principal geometries: $\underline{\rm I}$, tip magnetization parallel ($\vec{m}_{\rm tip} \uparrow\uparrow \vec{S}_D$) or antiparallel ($\vec{m}_{\rm tip} \uparrow\downarrow \vec{S}_D$) to the domain magnetization $\vec{S}_D$; $\underline{\rm II}$, tip magnetization parallel ($\vec{m}_{\rm tip} \uparrow\uparrow \vec{S}_{\rm DW}$) or antiparallel ($\vec{m}_{\rm tip} \uparrow\downarrow \vec{S}_{\rm DW}$) to the DW magnetization $\vec{S}_{\rm DW}$; and $\underline{\rm III}$, out of the plane tip magnetization ($\vec{m}_{\rm tip} \odot \vec{S}_{xy}$) or an into the plane magnetization ($\vec{m}_{\rm tip} \otimes \vec{S}_{xy}$), which is perpendicular to $\vec{S}_D$ as well as to $\vec{S}_{\rm DW}$. During the simulation the tip has been moved at a constant height $h = 2a$ along the stripe (in $+x$ direction). All our calculations correspond to the experimental constant-height mode [6]. The time dependence of the DW displacement $\Delta x_{\rm DW}$ for the three scenarios is plotted in Fig. 2. Black or gray (red) solid curves correspond to the possible orientations of the tip magnetization in scenarios $\underline{\rm I}$–$\underline{\rm III}$, while the dashed line represents the position of the tip.

In the first scenario ($\underline{\rm I}$) the tip magnetization is collinear with the domain magnetization $\vec{S}_D$. The spin torque is minimal above the domains for both cases, since the angle θ between the tip magnetization and the magnetic moment of the atoms underneath the tip is π for $\vec{m}_{\rm tip} \uparrow\uparrow \vec{S}_D$ or 0 for $\vec{m}_{\rm tip} \uparrow\downarrow \vec{S}_D$. When the tip reaches the DW, the spin torque increases because of the noncollinearity of the magnetization in the DW ($\pi > \theta > 0$). As the atoms in the DW are weaker coupled to their neighbors than those in the domains (their exchange energy is higher), the spin torque effectively aligns the magnetic moments in the direction of the tip magnetization. The spin torque is transformed into the kinetic energy leading to a DW motion, which decreases to zero when the minimum of the internal energy is reached. For $\vec{m}_{\rm tip} \uparrow\uparrow \vec{S}_{\rm D}$ geometry [black curve in Figs. 2 ($\underline{\rm I}$ a) and 2 ($\underline{\rm I}$ b)], the spin torque orients the underlying moments along the $+x$ direction and leads to a motion of the DW in the same direction. Hence, the tip pushes the wall ahead. In the case of $\vec{m}_{\rm tip} \uparrow\downarrow \vec{S}_D$ [gray (red) curve], the spin torque orients the underlying moments

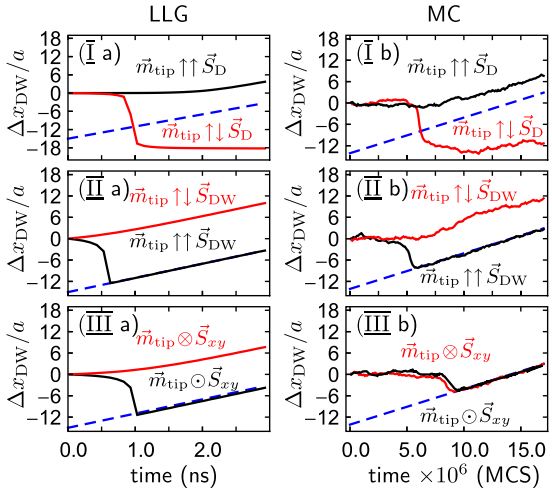

FIG. 2 (color online). Domain wall displacement $\Delta x_{\rm DW}$ of a ferromagnetic stripe versus time. Results of spin dynamics (LLG) and of MC simulations (MC). The tip moves with constant velocity marked by the dashed line. ($\underline{\rm I}$ a) and ($\underline{\rm I}$ b) for a tip magnetization pointing parallel and antiparallel to the initial domain $\vec{S}_D$, ($\underline{\rm II}$ a) and ($\underline{\rm II}$ b) parallel and antiparallel to the DW orientation $\vec{S}_{\rm DW}$, and ($\underline{\rm III}$ a) and ($\underline{\rm III}$ b) pointing into or out of the plane.

along the $-x$ direction, as the tip magnetization points along the same direction. To achieve an equilibrium position again the DW moves in the $-x$ direction until the torque vanishes. Since the tip itself moves in the opposite direction ($+x$), the contact to the wall is lost. To gain better understanding of the described behavior and make a link to the experiments, we analyzed the experimentally accessible spin dependent tunneling conductivity G_{sp}. The conductivity of a tunnel junction between two ferromagnetic electrodes (tip and sample in our case) is proportional to the scalar product $G_{sp} = \vec{S}_{tip} \cdot \vec{S}_i$ [9,16]. It is maximal for the parallel ($\theta = 0$) and minimal for the antiparallel ($\theta = \pi$) magnetization of the two electrodes. In the spin-resolved spectroscopic mode of SP-STM experiments [6], the dI/dU curves correspond to the position dependent changes in the conductivity $G_{sp}(\vec{r}_{tip})$. As all information on $G_{sp}(\vec{r}_{tip})$ in our calculations is incorporated into the s-d Hamiltonian [Eq. (3)], we are able to calculate $G_{sp}(\vec{r}_{tip}) \propto \langle g\vec{\mathcal{T}}_i \vec{S}_i \rangle$ and, hence, predict $G_{sp}(\vec{r}_{tip}) \sim I/U$.

Conductivity curves for scenario $\underline{\mathrm{I}}$ are plotted in Fig. 3 ($\underline{\mathrm{I}}$). In the $\vec{m}_{tip} \uparrow\uparrow \vec{S}_D$ geometry (black circles), G_{sp} is maximal above the initial domain ($\theta = 0$). When the tip reaches the DW, the conductivity does not change, because the DW is pushed ahead in $+x$ direction, keeping θ close to zero. The oscillations originate from the atomic resolution of our simulations. For $\vec{m}_{tip} \uparrow\downarrow \vec{S}_D$ (red rectangles), G_{sp} is minimal above the initial domain ($\theta = \pi$). Approaching the DW, G_{sp} increases due to a motion of the DW towards the tip and finally underneath the tip. In order to retain this energetically favorable situation, the tip loses contact and moves further across the domain magnetized parallel to the tip magnetization, keeping G_{sp} maximal ($\theta = 0$). A characteristic shape of the $G_{sp}(\vec{r}_{tip})$ as well as Δx dependencies permits us to make a clear conclusion about the dynamical regime of the DW manipulation (pushing or pulling).

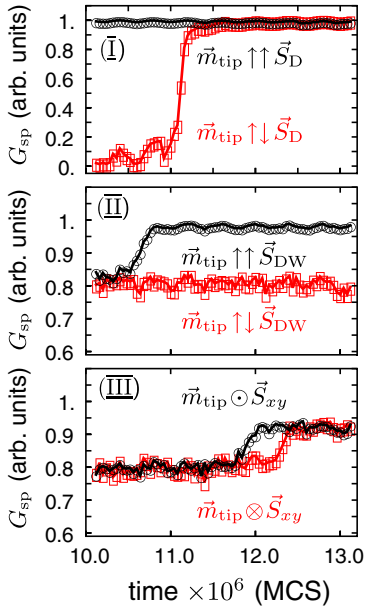

FIG. 3 (color online). Spin dependent conductivity versus time for the different tip magnetizations.

In the second scenario ($\underline{\underline{\mathrm{II}}}$), the tip is magnetized perpendicularly to the domains, i.e., parallel ($\vec{m}_{tip} \uparrow\uparrow \vec{S}_{DW}$) or antiparallel ($\vec{m}_{tip} \uparrow\downarrow \vec{S}_{DW}$) to the DW. In the case of $\vec{m}_{tip} \uparrow\uparrow \vec{S}_{DW}$ [black curve in Figs. 2 ($\underline{\underline{\mathrm{II}}}$ a) and 2 ($\underline{\underline{\mathrm{II}}}$ b)], the spin torque is maximal when the tip is above the domains ($\theta = \pi/2$) and minimal above the DW ($\theta = 0$). When the tip approaches the DW, the magnetic moments underneath the tip rotate in the $+y$ direction. As a result, the DW moves towards the tip until it remains directly underneath it minimizing the spin torque. For $\vec{m}_{tip} \uparrow\downarrow \vec{S}_{DW}$ geometry [gray (red) curve in Figs. 2 ($\underline{\underline{\mathrm{II}}}$ a) and 2 ($\underline{\underline{\mathrm{II}}}$ b)], the spin torque is maximal when the tip is above the domains ($\theta = -\pi/2$) and minimal above the DW ($\theta = \pi$). In the neighborhood of the DW the spin torque aligns the magnetization in the $-y$ direction, which leads to a repulsion of the DW away from the tip. Hence, in scenario $\underline{\underline{\mathrm{II}}}$ two different manipulation modes can be identified. In the former case ($\vec{m}_{tip} \uparrow\uparrow \vec{S}_{DW}$) the tip is situated above the center of the DW, pulling it, and in the latter case ($\vec{m}_{tip} \uparrow\downarrow \vec{S}_{DW}$) pushing it ahead. When using this knowledge for the interpretation of the achieved conductivity curves [Fig. 3 ($\underline{\underline{\mathrm{II}}}$)], it becomes clear that G_{sp} increases while the tip crosses the wall for $\vec{m}_{tip} \uparrow\uparrow \vec{S}_{DW}$ (black circles) and subsequently remains constant when pulling the DW. Loss of a contact between the tip and the DW leads to a drop in the conductivity; see [17]. For $\vec{m}_{tip} \uparrow\downarrow \vec{S}_{DW}$ [red rectangles in Fig. 3 ($\underline{\underline{\mathrm{II}}}$)], the conductivity remains unchanged as the wall is pushed.

In the last scenario $\underline{\underline{\underline{\mathrm{III}}}}$ the tip magnetization points into ($\vec{m}_{tip} \otimes \vec{S}_{xy}$) or out of the plane ($\vec{m}_{tip} \odot \vec{S}_{xy}$). The spin torque acting on the magnetization in the domains and the DW is equal. However, due to the weak exchange coupling of the magnetic moments in the DW, the DW magnetization is more easily influenced by the spin torque. The absolute minimum of the energy for $\vec{m}_{tip} \otimes \vec{S}_{xy}$ as well as for $\vec{m}_{tip} \odot \vec{S}_{xy}$ is the configuration with the DW directly underneath the tip. For this reason, in the MC simulations the DW is attracted by the tip and then remains underneath it until the end of a scan [Fig. 2 ($\underline{\underline{\underline{\mathrm{III}}}}$ b)] if the current is sufficient to align magnetic moments in the center of the DW into the hard axis. Hence, the DW is pulled by the tip in both cases. In the spin dynamic procedure a tip with an out of the plane magnetization pulls the DW, while an into the plane magnetization pushes the DW ahead; see Fig. 2 ($\underline{\underline{\underline{\mathrm{III}}}}$ a). The main role for this behavior is the first term of Eq. (2) used in the spin dynamic calculations. This term requires a clockwise rotation of the magnetization with respect to the effective field $\vec{H}_i$. The spin torque [the fourth term of Eq. (2)] tries to

align the magnetization of the sample along the hard axis. In order to avoid this energetically unfavorable situation the DW moves along the x axis. In the MC simulation a system always goes towards the minimum of the total energy. The way the system does it is arbitrary. In the spin dynamics, however, the kinetic energy of the second term of Eq. (2) leads to a motion of the wall away from the tip ($+x$ direction) for $\vec{m}_{\mathrm{tip}} \otimes \vec{S}_{xy}$, while the motion is towards the tip ($-x$ direction) for the $\vec{m}_{\mathrm{tip}} \odot \vec{S}_{xy}$ geometry. Therefore, the DW immediately finds the global minimum with zero torque for the $\vec{m}_{\mathrm{tip}} \otimes \vec{S}_{xy}$ geometry and remains in a local minimum for the $\vec{m}_{\mathrm{tip}} \odot \vec{S}_{xy}$ geometry (pushing mode). The different modes obtained in the framework of the two simulation methods for the $\vec{m}_{\mathrm{tip}} \otimes \vec{S}_{xy}$ geometry (pushing for spin dynamics and pulling from MC simulations) appear for currents strong enough to align magnetic moments into the hard axis only. The spin dependent conductivity derived from the MC simulations shown in Fig. 3 ($\underline{\underline{\mathrm{III}}}$) increases when the tip crosses the DW and then remains constant when pulling the DW, for both cases. The displacement between the two curves is due to thermal fluctuations in the MC simulations.

The results described above demonstrate that all tip-wall geometries discussed are applicable for the controlled manipulation of magnetic DWs. However, $\vec{m}_{\mathrm{tip}} \uparrow\downarrow \vec{S}_D$ geometry of scenario $\underline{\mathrm{I}}$ is cumbersome for manipulation, because the DW moves in opposite direction relative to the tip, before the tip loses contact with the wall. Furthermore, the scenarios $\underline{\mathrm{I}}$, $\underline{\underline{\mathrm{II}}}$, and $\underline{\underline{\mathrm{III}}}$ differ by the resulting mode of motion (pushing or pulling). From MC simulation we extract that v_c, the maximum possible tip velocity at which the sample is completely switched for a given I_0 and h, is larger in the pushing than in the pulling mode (2–4 times faster) [17]. At $v_{\mathrm{tip}} \approx v_c$ bending of the DW occurs as the DW does not succeed to relax at such high velocity. In principle the wall can be manipulated at v_c, but to achieve a wall relaxation we chose smaller velocities. However, one should mention that the equilibrium velocity is attained on time scales much smaller than the realistic speed of a STM tip.

Albeit the finding of faster switching in the pushing mode, the answer to the question about the optimal geometry for DW manipulation, is complex. While the $\vec{m}_{\mathrm{tip}} \uparrow\uparrow \vec{S}_D$ geometry is the fastest, it is impossible to reverse the sense of the DW motion without changing the tip magnetization. For $\vec{m}_{\mathrm{tip}} \uparrow\downarrow \vec{S}_{\mathrm{DW}}$ one can move the DW by approaching from either side, but for switching of the direction of motion, the tip has to be positioned on the other side of the DW. Operating in the pulling mode the DW follows the lateral motion of the tip; hence, the DW can be moved in both directions ($\pm x$) without changing the tip magnetization. The $\vec{m}_{\mathrm{tip}} \uparrow\uparrow \vec{S}_{\mathrm{DW}}$ geometry ensures the fastest switching in the pulling mode, as the spin torque in this case is minimal, while the tip-wall interaction strength is maximal. Manipulating a DW with a tip magnetization pointing along the hard axis is just possible for a weak hard axis anisotropy (as in our case) or with a high current. Therefore, the configuration $\vec{m}_{\mathrm{tip}} \uparrow\uparrow \vec{S}_{\mathrm{DW}}$ with the DW underneath the tip is probably the best for future applications. Our simulations have been performed for an idealized system without pinning effects. From the simulations we estimate that a coercive field of 0.1 T or more, created, e.g., by defects, would be sufficient to compensate the spin torque and prevent a successful DW manipulation at $T \leq 1$ K. This lower limit of a coercive field is of the same order of magnitude as typical pinning fields in ultrathin ferromagnetic films [18]. However, they can be successfully overcome by increasing temperature [19] or increasing current.

In conclusion, the DW manipulation by a SP-STM tip has been studied theoretically by means of spin dynamic and MC simulations. Both methods yield identical results except for scenario $\underline{\underline{\mathrm{III}}}$, which can be explained in the framework of the different simulation methods. It has been demonstrated that all tip-sample geometries are suitable for DW manipulation. An analysis of costs and benefits reveals the geometry with a tip magnetization parallel to the DW magnetization ($\vec{m}_{\mathrm{tip}} \uparrow\uparrow \vec{S}_{\mathrm{DW}}$) as the optimal one. The theoretical time and distance dependence of the spin dependent conductivity G_{sp} shows characteristic features for each geometry studied and can be used in future experiments for identification of the corresponding manipulation modes.

Financial support from the DFG (SFB668-B3, B4) and from the Hamburgische Forschungs- und Wissenschaftsstiftung (Cluster of Excellence "Nanospintronics") is gratefully acknowledged.

[1] S. S. P. Parkin *et al.*, Science **320**, 190 (2008).
[2] M. Kläui *et al.*, J. Magn. **14**, 53 (2009).
[3] S. Allende *et al.*, J. Appl. Phys. **104**, 013907 (2008).
[4] A. Imre *et al.*, Physica (Amsterdam) **19E**, 240 (2003).
[5] T. Yamaoka *et al.*, Jpn. J. Appl. Phys. **45**, 2230 (2006).
[6] R. Wiesendanger, Rev. Mod. Phys. **81**, 1495 (2009).
[7] S. Krause *et al.*, Science **317**, 1537 (2007).
[8] R. Wieser *et al.*, Phys. Rev. B **82**, 144430 (2010).
[9] J. C. Slonczewski, J. Magn. Magn. Mater. **159**, L1 (1996).
[10] Z. Li and S. Zhang, Phys. Rev. B **68**, 024404 (2003).
[11] D. V. Berkov and N. L. Gorn, Phys. Rev. B **80**, 064409 (2009).
[12] L. Berger, Phys. Rev. B **54**, 9353 (1996).
[13] J. Tersoff and D. R. Hamann, Phys. Rev. B **31**, 805 (1985).
[14] G. Herzog *et al.*, Appl. Phys. Lett. **96**, 102505 (2010).
[15] S. Krause *et al.*, Phys. Rev. Lett. **103**, 127202 (2009).
[16] M. Jullière, Phys. Lett. **54**, 225 (1975).
[17] See Supplemental Material at http://link.aps.org/supplemental/10.1103/PhysRevLett.107.027203 for critical tip velocity.
[18] A. Lyberatos and J. Ferré, J. Phys. D **33**, 1060 (2000).
[19] A. Kirilyuk and J. Ferré, IEEE Trans. Magn. **29**, 2518 (1993).